Frother-Assisted Flotation of Different Origin Pyrites

Kamil MILEWSKI[1)], Jan DRZYMALA[2)]

[1)] Department of Geoengineering, Mining and Geology, Wroclaw University of Science and Technology, Wybrzeze Wyspanskiego 27, Wroclaw, Poland
[2)] Politechnika Wrocławska, Wydział Geoinżynierii, Górnictwa i Geologii, Wybrzeże Wyspiańskiego 27, 50-370 Wrocław, Poland; email: jan.drzymala@pwr.edu.pl

http://doi.org/10.29227/IM-2019-02-25

Submission date: *30-09-2019* | Review date: *22-10-2019*

Abstract

Hallimond tube flotation of different origins pyrites (coal-derived, Rio Tinto and Huanzala) and copper –bearing shale, having different hydrophobicities determined by contact angle, were investigated in water and aqueous solutions of butyl diethylene glycol ether. Pyrites flotation depended on hydrophobicity, particle size fraction and frother concentration. Three regions of the yield-frother concentration plot were distinguished: Jones-Ray region at low frother concentration with decreasing yield due to entopic effects, Lyster region at medium frother concentration with increasing yield due to decreasing film stability and Zisman region at high frother concentration with decreasing yield due to surface tension drop. The flotation kinetics in the form of 1st order specific rate, equal to the kinetic constant, was similar for all three pyrites and was equal to 0.032±0.002 min^{-1}, while their yield after 45 min flotation was dependent on pyrite origin.

Keywords: flotation, pyrite, sulphide, shale, Hallimond tube, butyl diethylene glycol ether, C_4E_2

1. Introduction

Collectorless frother-assisted flotation is used when there is a need to remove naturally hydrophobic components of ores or raw materials that interferes with subsequent collector flotation of a valuable minerals Such approach is used for instance for separation of carbonaceous matter and pyrite from chalcopyrite (Pokrajcic et al., 2005), carbonaceous matter from lead and zinc sulfides (Shanthaveerappa et al., 1995, Smith et al., 2008; Burgess et al., 2003; Jalilian et al. 2014), carbonaceous shale from copper sulfides (Konieczny et al., 2013). The removal of selected components before proper flotation is called pre-flotation (Wills and Napier-Munn, 2006; Pokrajcic et al., 2005). Pre-flotation is performed in the presence of only frother. The applied frother is either a single organic foaming agent, a mixture of organic frothers, or organic frothers in saline waters. Sometimes frother-only flotation is performed as the main process. It takes place during graphite flotation (Pugh, 2000).

Although the foundations of the pre-flotation seem to be simple, it still requires investigations to better understand the process, especially when there a co-flotation of unwanted components, as in the case of carbonaceous matter/pyrite/chalcopyrite system (Pokrajcic et al., 2005). The aim of this paper is shed some more light on pre-flotation involving pyrite. Since the natural hydrophobicity of sulfides depends on their origins (Lekki and Drzymala, 1990; Bulatovic, 2007), the collectorless frother-assisted flotation of three pyrites of different origins were investigated in a wide range of concentrations of butyl diethylene glycol ether frother. For comparison purpose, copper-bearing carbonaceous shale, having similar to pyrites hydrophobicity but much lower density, was also tested. The flotation experiments were performed in a elongated Hallimond tube to reduce the entrainment of particles.

2. Experimental

Coal-derived, Huanzala and Rio Tinto pyrites were used in the investigations. Coal pyrite (Fig.1a) was obtained from a coal mine located in Lower Silesia in Poland. Rio Tinto pyrite was from the Iberian Pyrite Belt in Spain and was mostly in the form of intergrown cubes (Fig. 1b) while Huanzala pyrite originated from Peru and was in the form of monocrystalline cubes (Fig.1c). Used in the experiments Kupferschiefer shale came from the Legnica-Glogow Copper District in Lower Silesia, Poland (Fig. 1d). Its composition was 0.83% Cu, 5.3% Corg and 30.1% CO_2.

The mineral samples were crushed either with a jaw crusher (shale) or manually with a hammer (pyrites). Next, the samples were sieved using metal screens with a mesh size of 0.2 mm, 0.1 mm, 0.075 mm and 0.06 mm to produce 0.2–0.1, 0.1–0.075, 0.075–0.06 and -0.06 mm particle size fractions. In each flotation test a 2.5 g sample of solids was used. Flotation tests were carried out in an elongated Hallimond tube. Its total high was 36 cm, volume 210 cm^3 and diameter of the glass tube 25 mm. The air flow was 19 cm^3/min. Aqueous solutions of 99% pure butyl diethylene glycol ether (C_4E_2) frother were used in the experiments. C_4E_2 was purchased from Sigma-Aldrich.

A sample of the solids were made wet with aqueous solution of frother in a beaker and next transferred to the Hallimond tube. Flotation was performed with air. The yield of flotation was read off from the receiver of the Hallimond tube which was calibrated in the 0–100% yield scale. The total flotation time was 45 minutes. Flotation experiments for Kupferschiefer shale were made twice for each particle size due to the greater amount of material available and to verify the results of the flotation. The results of two flotation tests for the same particle size fraction of shale were made averaged.

Fig. 1. Photographs of investigated materials. a) coal pyrite, b) Rio Tinto pyrite, c) Huanzala pyrite, d) shale
Rys. 1. Fotografie badanych materiałów. a) piryt węglowy, b) Rio Tinto, c) Huanzala, d) łupek

Tab. 1. Density and contact angles of aqueous solutions of C_4E_2 frother on surfaces of pyrites and shale
Tab. 1. Gęstość i kąt zwilżania wodnych roztworów spieniacza C_4E_2 na powierzchni pirytów i łupka

Solid	Density g/cm³	Contact angle for C_4E_2 frother concentration (g/dm³)					
		0	0.1	0.5	1.0	2.5	5.0
Coal-pyrite	4.8-5.0*	-	3	6	9	-	-
Rio Tinto pyrite	4.8-5.0*	-	17	22	28	-	-
Huanzala pyrite	4.8-5.0*	20	24	30	32	28	26
Shale	2.4-2.7**	-	23	29	33	-	-

* CRC, 1986/7, **Cependa et al., 2014

The angle of contact between water drop and solid surface was measured by taking into account the height and radius of contact of the sessile drop with the solid surface. The flat and smooth parts of the investigated materials were selected and washed several times with distilled water and finally polished with papers cloth until shining before contact angle measurements.

3. Results

Pyrites and shale used in the investigations differed in hydrophobicity and density. Their hydrophobicity, characterized but contact angle along with density are given in Table 1.

It results from Table 1. that the hydrophobicity of pyrites depend on their origin, which is a known phenomenon (Bulatovic, 2007). The hydrophobicity of the investigated solids increases in the following order: coal-derived, Rio Tinto, Huanzala pyrites and finally shale. Coal-pyrite was very weakly hydrophobic with contact angle only a few degrees while the contact angles of the remaining solids were greater being in the vicinity of 20 degrees. In literature, the contact angle of pyrites are usually greater, that is from 35 (Wang et al., 1991) to 87 (Koval and Matysek, 2014) degrees. The contact angles of investigated pyrites were slightly increasing with the frother concentration in the investigated range of 0.1–1.0 g/cm³ of aqueous solution of frother.

Different size fractions of pyrites and shale were subjected to flotation tests and the results, in the form of yield as a function of flotation time, are given in Fig. 2.

4. Discussion of results

Shown in Fig. 2 flotation kinetics curves are a useful source of information on properties of the investigated frother aqueous solution/mineral particles/gas system including influence of frother concentration, particle size and hydrophobicity on flotation and its rate. These issues will be discussed in the following sections of the paper.

4.1. Influence of frother concentration on flotation

The obtained kinetics plots can be transformed into incentive curves (Drzymala, 2018), which relate either yield maximum, or yield after a certain time of flotation, and the incentive parameter regulating the process. In our case the incentive parameter is the concentration of frother. The relations between yield of the investigated pyrites and shale after 45 minutes of flotation in C_4E_2 frother aqueous solutions for different size fractions of the solids are given in Fig. 3.

The incentive curves show that the smaller size of the particles the greater yield and that the curves form different maxima and minima. To create a more general view of the shape of the incentive curves for the investigated solids Fig. 3. was replotted separately for each particle size fraction for all investigated solids. The outcome is presented in Fig. 4.

Now, it is possible to distinguish three yield regions in the incentive curves. At low frother concentration, between zero and 0.1 g/dm³, there is a small decrease of the yield. Such yield drops were observed in many studies, mostly during flotation in salty solutions (Laskowski, 1963; Chin and Somasundaran, 1993). This drop can be assigned to a change in the electrical double layer structure and is of entro-

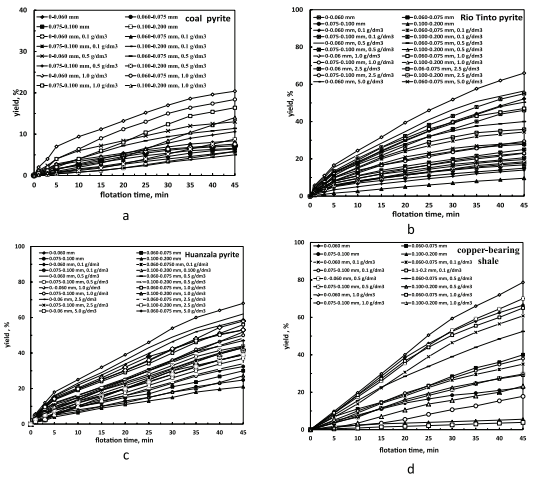

Fig. 2. Flotation kinetics curves of investigated pyrites and shale a) coal pyrite, b) Rio Tinto pyrite, c) Huanzala pyrite, d) shale
Rys. 2. Krzywe kinetyki flotacji badanych pirytów i łupka a) piryt węglowy, b) Rio Tinto, c) Huanzala, d) łupek

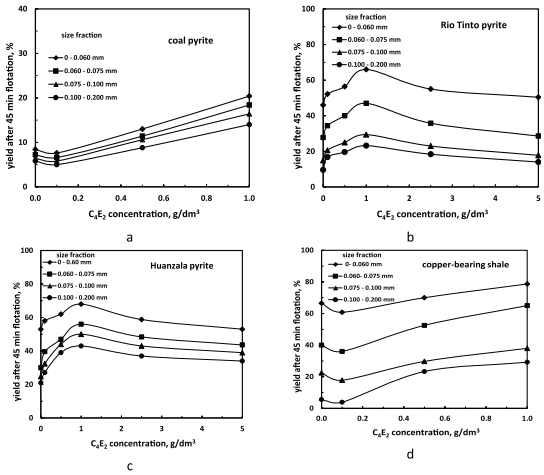

Fig. 3. Incentive curves relating yield and frother concentration for different size fractions of investigated solids
a) coal pyrite, b) Rio Tinto pyrite, c) Huanzala pyrite, d) shale
Rys. 3. Krzywe bodźcowe wiążące wychód i stężenie spieniacza dla różnych klas ziarnowych badanych substancji
a) piryt węglowy, b) Rio Tinto, c) Huanzala, d) łupek

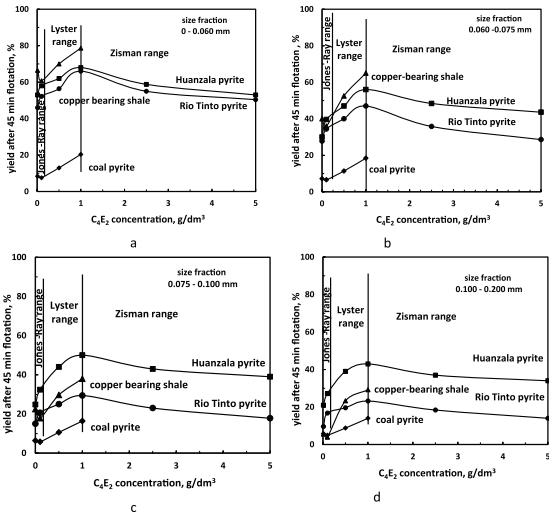

Fig. 4. Incentive curves relating yield and applied frother C_4E_2 concentration for different size fractions of investigated solids.
Size fractions: a) 0–0.060, b) 0.060–0.075, c) 0.075–0.100, d) 0.100–0.200 mm
Rys. 4. Krzywe bodźcowe wiążące wychód i stężenie spieniacza dla różnych klas ziarnowych badanych substancji.
Klasy ziarnowe: a) 0–0.060, b) 0.060–0.075, c) 0.075–0.100, d) 0.100–0.200 mm

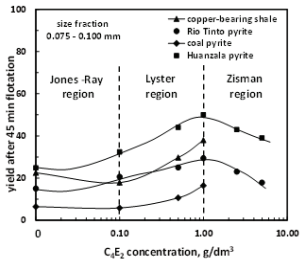

Fig. 5. Semi-logarithmic incentive curves relating yield and concentration of frother for selected (0.075–0.100 mm) size fractions of investigated solids indicating three (Jones-Ray, Lyster and Zisman) flotation regions

Rys. 5. Półlogarytmiczne krzywe bodźcowe wiążące wychód i stężenie spieniacza dla wybranych klas ziarnowych badanych substancji (0.075–0.100 mm) wskazujące trzy zakresy flotacji (Jonesa-Raya, Lystera oraz Zismana)

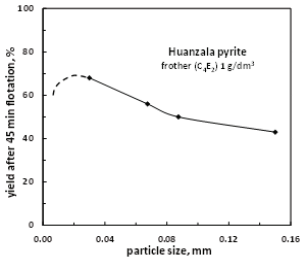

Fig. 6. Yield of Huanzala pyrite in the presence of 1.0 g/dm³ C_4E_2 frother as a function of average particle size (each size fraction was subjected to flotation separately)

Rys. 6. Wychód pirytu Huanzala pirytu w obecności 1.0 g/dm³ spieniacza C_4E_2 w funkcji średniego rozmiaru ziaren (każda frakcja była flotowana osobno)

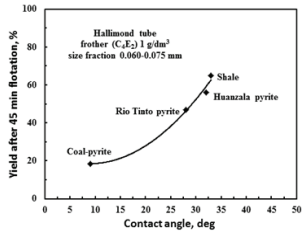

Fig. 7. Yield versus contact angle of pyrites and shale at frother concentration equal to 1g/dm³

Rys. 7. Wychód od kąta zwilżania dla pirytów oraz łupka przy stężeniu spieniacza 1g/dm³

pic origin (Deschênes et al., 2017). Such a phenomenon was noted by Jones and Rey (1937) during measuring the surface tension of certain salts in water. Therefore, this area in our work is called the Jones-Ray region.

After a small decrease, the yield increases with increasing frother concentration. We can be called the Lyster region, to honor Lyster as a great inventor who was first to use frothers in flotation (Lynch, 2007). There is no a simple explanation of the phenomenon of yield increase with increasing frother concentration. According to Pugh (2007) small particles have difficulties to collide with large bubbles in their journey in the streamlines around the rising bubble. Frother reduce the size of bubbles. Therefore, flotation kinetics increases as the bubbles size decreases and their population also increases (Laskowski 1998). Another factor is the stability of a complex thin film existing between a colliding particle and a bubble (Szczerkowska et al. 2017). The film consists of nano-bubbles (foam film) from the solid surface side and the adsorbed frother from the bubble side. This film seems to be less stable in the presence of frother. According to Krasowska et al. (2003) without surfactant the attachment of even highly hydrophobic tetrafluoroethylen was severely hindered due to great stability of the film. More research is needed to get a better picture of flotation in the Lyster region.

Above the frother concentration equal to about 1.0 g/cm³, that is 6.2 mmol/dm³ of C_4E_2, the flotation yield decreases. The simplest explanation can be based on the effect investigated by Zisman (1964). He proved that surfactants that greatly lower surface tension of aqueous solution, make the solid less hydrophobic, until a full hydrophilicity, indicated by zero contact angle, is reached. The Zisman effect is well visible when contact angle θ is measured and cos θ vs. surface tension (Lyklema, 2000) is plotted. Thus, the area of yield drop caused by excessive amounts of frother can be called the Zisman region.

The three regions of the yield/frother concentration relation are well visible in the incentive plot in the semi-logarithmic form (Fig. 5).

4.2. Influence of particle size and density on flotation

Previously shown Figs 4a-d revealed the influence of particle size and density on yield. For the investigated solids the yield increases with decreasing particle size. Figure 6 presents, for example, this relation for Huanzala pyrite floated at 1.0 g/dm³ of C_4E_2 frother.

The yield of flotation in a Hallimond tube is sensitive not only to particle size but also density. The density of natural

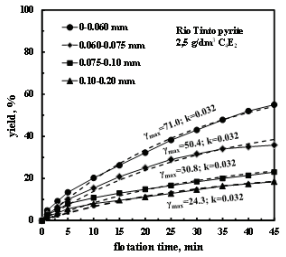

Fig. 8. Kinetics curves of flotation of different size fractions of Rio Tinto pyrite approximated (dashed line) with first order kinetic equation (Eqs 1 and 2)
Rys. 8. Krzywe kinetyczne flotacji różnych klas ziarnowych pirytu Rio Tinto aproksymowane (linia przerywana) równaniem kinetyki 1-szego rzędu (równania 1 oraz 2)

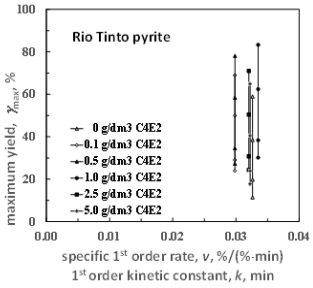

Fig. 9. Limits (γ_{max} vs v = k) curves for flotation of different size fraction of Rio Tinto pyrite. Average k is 0.032±0.002
Rys. 9. Krzywe limitów (γ_{max} vs v = k) dla flotacji różnych klas ziarnowych pirytu Rio Tinto. Średnie k wynosi 0.032±0.002

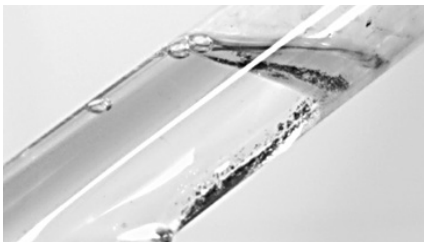

Fig. 10. Upper part of the Hallimond tube with floating RioTinto pyrite (size fraction 0.075–0.1 mm, 1.0 g/dm³ C_4E_2). Flotation is slow due to small coverage of bubbles with pyrite as indicated by dashed line around a selected bubble
Rys. 10. Górna część aparatu Hallimonda z flotującym pirytem RioTinto (frakcja 0.075–0.1 mm, 1.0 g/dm³ C_4E_2). Flotacja jest wolna z powodu nikłego pokrycia pęcherzyków pirytem, co wskazano linią przerywaną wokół wybranego pęcherzyka

pyrites is between 4.8 and 5.0 (Manecki, 2004). For pure the density of FeS_2 is 5.0 g/cm³ (CRC, 1986/7) while the density of the investigated shale was 2.6 g/cm³. Thus, the density of pyrite in water, equal to 3.9 g/cm³, is more than two-fold greater than that of shale (1.6 g/cm³). Inspection of Figs 4a-d indicates, that yield of shale increases with decreasing particle size much more than that of pyrites. This is so because shale is less dense than pyrite and much more subjected to entrainment which always is accompanying flotation in the Hallimond tube.

4.3. Influence of hydrophobicity on flotation yield

The hydrophobicities of the investigated pyrites, measured as contact angle, were shown in Table 1. They were small, but not identical. The contact angles of pyrites measured by the sessile aqueous drop, for instance containing 1.0 g/cm³ (6.2 mmol/dm³) of frother, were: coal-derived 9°, Rio Tinto 28°, Hunazala 32°, shale 33°. The yield of flotation correlates well with the contact angle of the investigated solids (Fig. 7.).

4.4. Kinetics of flotation

Kinetics is an important aspect of flotation. To check how hydrophobicity of the investigated pyrites influences flotation kinetics, the original flotation data from Fig. 1 were approximates with 1st order kinetic equation, which in the derivative form is

$$\frac{\frac{d_y}{d_t}}{(\gamma_{max}-\gamma)} = v \tag{1}$$

while in the integral form

$$\gamma = \gamma_{max}(1-e^{-kt}) \tag{2}$$

where k is the 1st order kinetic constant while v is the 1st order specific rate. The unit of k is 1/min because it concerns the amount of matter in concentrate (γ and γ_{max}) while v has the unit of g/(g·min) (or %/(%·min) because it deals with the matter in concentrate and in the tailing. The numerical values of γ and k are identical: num k = num v, where abbreviation num stands for numerical value (Drzymala et al., 2017).

Figure 8 shows, as an example, the 1st order kinetics of Rio Tinto pyrite flotation while Fig. 9 provides relation between calculated γ_{max} and v = k.

It appears, that to a great extent, the specific rate of flotation between the flotation starting point and maximum

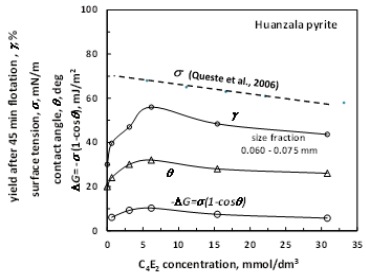

Fig. 11. Comparison of investigated flotation system parameters leading to flotation yield (γ) and change of Gibbs potential of flotation ΔG where ΔG=σ(1-cosθ). Surface tension data of C4E2 frother was taken from Queste et al. (2006)

Rys. 11. Porównanie wybranych parametrów badanych układów flotacyjnych wpływających na wychód flotacyjny (γ) oraz zmiany potencjału flotacji Gibbsa ΔG gdzie ΔG=σ(1-cosθ). Napięcie powierzchniowe dla C4E2 zaczerpnięto z pracy Queste et al. (2006)

yield does not change with the concentration of the frother. In addition, the specific rate is similar for all three pyrites and is equal to 0.032±0.002 %/(%·min). The flotation specific 1st order rate of shale is slightly lower and amounts 0.026±0.002 %/(%·min). These data indicate that hydrophobicity of the investigated solids does not influence the rate of the process but effects the maximum yield.

5. Conclusions

Our investigations confirmed that pyrites of different origins have different hydrophobicity measured by contact angle. The contact angles of coal-derived, Rio Tinto and Huanzala pyrites, measured in aqueous 1 g/dm³ C_4E_2 solution were 9, 28 and 32 degrees, respectively. Flotation of the pyrites and carbonaceous shale, investigated for comparison purpose, depended on hydrophobicity, particle size fraction and frother concentration. Three regions for the yield-frother concentration relation can be distinguished: Joney-Ray region at low frother concentration with decreasing yield due to entopic effects, Lyster region at medium frother concentration with increasing yield due to decreasing film stability and Zisman region at high frother concentration with decreasing yield due to surface tension drop. The flotation kinetics for all three pyrites was slow and similar (0.032±0.002 min^{-1}) while their recovery after 45 min flotation was different and depended on the pyrite origin. Slow flotation was a results of very small coverage of air bubbles with pyrite (Fig. 10).

It results from our investigations that the increase of yield (γ) in the Lyster region (1–7 mmol/dm³) is caused by the increasing contact angle (θ) facilitated by frother while yield decreasing in the Zisman region (7–32 mmol/dm³) is governed by decreasing both surface tension (σ) and contact angle (Fig. 11). The yield of flotation well correlates with the change of the Gibbs potential of flotation (ΔG).

Acknowledgements

Preparation of this paper was financed by the Polish Government Statutory Research Grant No. 0401/0129/17.

Literatura – References

1. Bulatovic, S.M., 2007. Handbook of Flotation Reagents. Chemistry, Theory and Practice Flotation of Sulfide Ores, Elsevier, Amsterdam
2. Burgess, F, Reemeyer, L, Spagnolo, M, Ashley, M and Brennan, D, 2003. Ramp up of the Pasminco Century Concentrator to 500 000 tpa zinc metal production in concentrate, in Proceedings Eighth Mill Operators' Conference, pp 153-163, the Australasian Institute of Mining and Metallurgy: Melbourne)
3. Cependa, K., Drzymala, J., Lewicka, M.P., 2014. Gęstość łupka miedziowego, in: Łupek miedzionośny, Drzymała J., Kowalczuk P.B. (red.), WGGG PWr, Wrocław, 2014, 19-21
4. Chin, L.; Somasundaran, P., 1993. Role of electrical double layer forces and hydrophobicity in coal flotation in NaCl solutions, Energy Fuels, 7, 244.
5. CRC Handbook of chemisty and physics, 67th ed., 1986/7, CRC Press, Boca Raton
6. Deschênes, L., Lyklema, J., St-Germain, F., 2017. Entropy of aqueous surfaces. Application to polymeric Langmuir films. Adv. Colloid Interface Sci. 247:149-162
7. Drzymala, J., 2018. Evaluation of flotation reagents by normalization procedures, Physicochem. Probl. Miner. Process., 54(1), 182-192
8. Drzymala, J., Ratajczak, T., Kowalczuk, B.P., 2017. Kinetic separation curves based on process rate considerations, Physicochem. Probl. Miner. Process, 53(2), 983-995
9. Jalilian, H., Shafaei, S.Z., Noparast, M., Haghi, H., 2014. Reduction of lead and zinc loss in preconcentration process of Koushk flotation circuit, Proceedings of 14th International Mineral Processing Symposium Turkey, 2014, 379-384
10. Jones G., Ray W. A., 1937. The surface tension of solutions on electrolytes as a function of the concentration. I. A differential method for measuring relative surface tension, J. Am. Chem. Soc., 59, 187-198
11. Konieczny, A., Pawlos, W., Krzeminska, M., Kaleta, R., Kurzydlo, P., 2013. Evaluation of organic carbon separation from copper ore by pre-flotation, Physicochem. Probl. Miner. Process. 49(1), 189–201
12. Koval, L., Matysek, D., 2014. Evaluation of contact angle on pyrite surface, Journal of the Polish Engineering Society, 2(34), 119-126
13. Krasowska, M., Krzan M., Malysa K., 2003. Bubble collisions withhydrophobic and hydrophilic surfaces in α-terpineol solutions, Physicochemical Problems of Mineral Processing, 37, 37-50
14. Laskowski J., 1998. Frothers and frothing, w: Frothing in Flotation II, J.S. Laskowski, E.T. Woodburn (eds.), Gordon and Breach, Australia, 1-49
15. Laskowski, J., 1963. Mechanism of inorganic salts action in coal salt flotation process, Ph.D. thesis, Silesian Technical University, Gliwice, Poland, in Polish
16. Lekki, J., Drzymala, J., 1990. Flotometric Analysis of Collectorless Flotation of Sulfide Materials, Colloids and Surfaces, 44, 179-190
17. Lyklema J., 2000. Fundamentals of interface and colloid science. Vol. III, Liquid-liquid interfaces, Academic Press, London.
18. Lynch, A.J., Watt, J.S., Finch, J.A., Harbort, G.E., 2007. History of flotation technology. In Froth flotation: A century of innovation, M.C. Fuerstenau, G.J. Jameson, R.-H Yoon Eds., SMME Inc., Littleton
19. Manecki, A., 2004. Encyklopedia mineralow, Uczelniane Wydawnictwa Naukowo-dydaktyczne, Krakow
20. Pokrajcic, Z., Harbort, G J, Lawson V., Reemeyer, L., 2005. Applications of the Jameson Cell at the head of base metal flotation circuits, in: Centenary of Flotation Symposium, Brisbane, Queensland, 6–9 June 2005 (The Australasian Institute of Mining and Metallurgy: Melbourne, 165–170
21. Pugh, R.J. 2007. The physics and chemistry of frothers. In Froth Flotation:A Century of Innovation; Fuerstenau, M.C., Jameson, G., Yoon, R.H., Eds.; SME: Englewood, CO, USA, 259–281.
22. Pugh, R.J., 2000. Non-ionic polyethylene oxide frothers in graphite flotation, Minerals Engineering, 13(2), 151-162
23. Queste S., Bauduin, P., Touraud D., Kunz, W., Aubry J-M., 2006, Short chain glycerol 1-monoethers - a new class of green solvo-surfactants, Green Chem., 8, 822-830
24. Shanthaveerappa, S.C., Sharma, N.K., Tamekar, G.G., Ravindranath, K., 1995. A comprehensive investigation on Rajpura-Fariba 60:40 calc silicate: graphite mica schist ore, in: Proc. Conf. honoring Prof. Kapur, Indian Institute of Technology, Kanpur, Dec. 11-15, 1995, Allied Pub., New Delhi

25. Smith, T., Lin, D., Lacouture, B., Anderson, G., 2008. Removal of Organic Carbon with a Jameson Cell at Red Dog Mine, Proceedings of the 40th Annual Canadian Mineral Processors Conference, Ottawa, Ontario, 22–24 January 2008, paper 21
26. Szczerkowska, S., Wiertel-Pochopien, A., Zawala, J., Larsen, E., Kowalczuk, B.P., 2017. Kinetics of froth flotation of naturally hydrophobic solids with different shapes, Proc. Flotation '17, November 13-16, 2017, Cape Town, South Africa
27. Wang X-H, Leonard, J.W, Parekh, B.K., Raichur, A.M., Jiang, Ch., 1991. Pyrite surface characterization and control for advanced fine coal desulfurization technology, March 1 – May 30 Progress Report, Department of Mining Eng. and Center for Applied Energy Research, University of Kentucky, Lexington
28. Wills, B.A., Napier-Munn, T.J., 2006. Mineral Processing Technology, 7th edition, Elsevier, Amsterdam
29. Zisman, W.A., 1964. Relation of the Equilibrium Contact Angle to Liquid and Solid Constitution, In: Contact Angle, Wettability, and Adhesion, , Adv. Chem. Ser., 43,1-55

Spieniaczowa flotacja pirytów różnego pochodzenia

W celce Hallimond poddano flotacji piryty różnego pochodzenia oraz łupek miedzionośny. Wśród pirytów były to piryt węglowy, Rio Tinto oraz Huanzala. Miały one różną hydrofobowość, którą mierzona jako kąt zwilżania dla wody i roztworów eteru butylowego glikolu dietylenowego. Spieniaczowa flotacja pirytu zależała od hydrofobowości, stężenia spieniacza oraz rozmiaru ziarn. Na wykresie wychód-stężenie spieniacza wyróżniono trzy zakresy flotacji: Jonesa-Raya przy niskim stężeniu spieniacza, gdzie zachodzi spadek wychodu wynikający z efektów entropowych, Lystera przy średnim stężenia spieniacza, gdzie zachodzi wzrost wychodu i zakres Zismana przy wysokiej koncentracji spieniacza powodującej obniżenie wychodu ze względu na spadek napięcia powierzchniowego. Kinetyka flotacji w postaci prędkości specyficznej 1-szego rzędu równa stałej kinetycznej 1-szego rzędu była podobna dla wszystkich trzech pirytów i wynosiła 0,032±0.002 min^{-1}, podczas gdy ich wychód po 45 minutach flotacji był uzależniony od pochodzenia pirytu.

Słowa kluczowe: flotation, pyrite, sulphide, shale, Hallimond tube, butyl diethylene glycol ether, C_4E_2